Progress In Electromagnetics Research, Vol. 109, 399–424, 2010

SEMI-ANALYTICAL SOLUTIONS OF THE 2-D HOMOGENEOUS HELMHOLTZ EQUATION BY THE METHOD OF CONNECTED LOCAL FIELDS

H.-W. Chang and S.-Y. Mu

Institute of Electro-optical Engineering, Department of Photonics
National Sun Yat-sen University, Kaohsiung 80424, Taiwan

Abstract—The frequency-domain finite-difference (FD-FD) methods have been successfully used to obtain numerical solutions of the two-dimensional (2-D) Helmholtz equation. The standard second-order accurate FD-FD scheme is known to produce unwanted numerical spatial and temporal dispersions when the sampling is inadequate. Recently compact higher-order accurate FD-FD methods have been proposed to reduce the spatial sampling density. We present a semi-analytical solution of the 2-D homogeneous Helmholtz equation by connecting overlapping square patches of local fields where each patch is expanded in a set of Fourier-Bessel (FB) series. These local FB coefficients correspond to a total of eight points, four on the sides and four on the corners of the square patch. The local field expansion (LFE) analysis leads to an improved compact nine-point FD-FD stencil for the 2-D homogeneous Helmholtz equation. We show that LFE formulation possesses superior numerical properties of being less dispersive and nearly isotropic because this method of connecting local fields merely ties these overlapping EM field patches which already satisfy the Helmholtz equation.

1. INTRODUCTION

In recent years hybrid FD-FD methods have been successfully applied to study many time-harmonic electromagnetic problems and even complex dielectric waveguide devices [1–9]. When combined with effective transparent boundary conditions such as the PML [10, 11] and the recently developed LM-TBC method [12], the hybrid FD-FD method can be quite computationally efficient for certain passive

Received 28 September 2010, Accepted 22 October 2010, Scheduled 3 November 2010
Corresponding author: Hung-Wen Chang (hchang@faculty.nsysu.edu.tw).

optoelectronic devices. The drawback of the FD-FD method is that one must solve for the resulting large sparse linear equation. Currently, no robust iterative linear equation solutions exist for the discretized FD-FD Helmholtz equation. As a result, FD-FD methods are rarely used for 3D applications. Under normal circumstances, the standard second-order FD-FD method requires at least 10 points per wavelength to discretize the Helmholtz equation in order to minimize unwanted numerical dispersion. Currently, high-order finite difference formulae are being developed [13–17] to reduce FD discretization density. First, a new approach based on 2-D scalar wave extrapolation leads to nine-point coefficients [13] for the FD-FD method. The illustration of the nine-point stencil is given in Fig. 1. The new formulation is derived from optimizing linear combination coefficients of two sets of standard five-point FD coefficients, one along the z-x axis and the other along the $z + x$ and $x - z$ axis. Immediately, we see that numerical anisotropy will be reduced with this new nine-point scheme covering eight propagating directions instead of the previous four. Furthermore, instead of using fixed coefficients for the Laplace operator, we can adjust and fine-tune the nine-point stencil for each given frequency to reduce temporal dispersion To lower the sampling density at high frequencies, there are also approaches based on fourth and sixth-order approximation of the 2D Helmholtz with an inhomogeneous source [14–17]. The advantages of these methods are that the frequency-dependent FD stencils are compact i.e., they do not involve points other than four side points and four corner points. Hence, direct inversion of the matrix equation from using a compact nine point stencil costs no more than those from using a standard five point stencil.

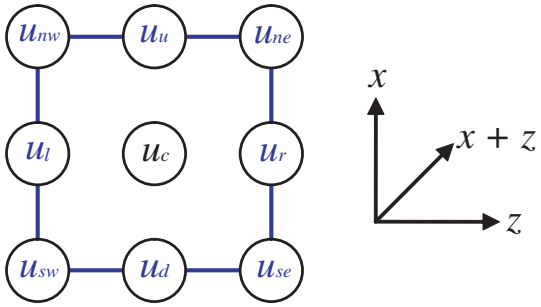

Figure 1. Compact 9-point array of grids consisting of the centered point u_c, four side points u_r, u_u, u_l, u_d and four corner points $u_{ne}, u_{nw}, u_{se}, u_{sw}$.

2. SUMMARY OF THE FD-FD METHODS

Since our method is related to existing FD-FD methods we shall briefly summarize the main results of various methods. Interested readers may also consult many fine textbooks [18–20] for additional information.

2.1. 1D Homogeneous Case

The 1-D homogeneous Helmholtz equation with z as the independent variable is given below

$$\left(\frac{d^2}{dz^2} + k^2\right) u(z) = 0. \tag{1}$$

Here, the constant k is the wavenumber, $k = 2\pi/\lambda$ where λ is the wavelength. Suppose that the unknown fields $\{u_i\}$, are evaluated at $z_i = i \cdot \Delta z$, for $i = \ldots, -1, 0, 1, \ldots$. We may approximate the second derivative of $u(z)$ by a second-order accurate finite-difference. Thus,

$$\frac{d^2}{dz^2} u(z) \cong \frac{1}{(\Delta z)^2} \left[u(z - \Delta z) - 2u(z) + u(z + \Delta z)\right]. \tag{2}$$

This will lead to the following 1-D FD equation for a given point u_0:

$$u_0 = \frac{1}{2 - (k\Delta z)^2} u_{-1} + \frac{1}{2 - (k\Delta z)^2} u_1. \qquad \text{(FD2-3)} \tag{3}$$

2.2. Classical Second-order Accurate 2D FD-FD Formulation

Referring to Fig. 1, the classical second-order accurate, five-point FD-FD stencil for this equation at point u_c is given by

$$u_c = \frac{u_r + u_u + u_l + u_d}{4 - k^2\Delta^2}. \qquad \text{(FD2-5)} \tag{4}$$

Here $\Delta = \Delta x = \Delta z$. Points u_r, u_u, u_l and u_d are side points of u_c located on the right, left, top (up) and bottom (down). Eq. (4) is denoted as FD2-5 where the fist digit is the order of accuracy and the second digit stands for total points involved in the given equation. Eq. (4) is known to be spatially dispersive in that the effective numerical wavenumber depends on the direction of propagation. Normally more than ten points per wavelength (typically fifteen to twenty) are needed to avoid excessive numerical dispersion. To simulate an integrated 2D optical device of several tens of wavelengths in each dimension requires significant memory and an up-to-date CPU. It is interesting to note that spatial dispersive can be reduced if one

carefully combines two standard five-point FD stencils, one along the x-z coordinates and another one along the rotated 45 degree x'-z' coordinates (using the corner points u_{ne}, u_{nw}, u_{se} and u_{sw}.)

$$\left(4 - k^2\Delta^2\right) u_c = \left(u_r + u_u + u_l + u_d\right), \qquad \text{(FD2-5+)} \tag{5}$$

$$\left(4 - 2k^2\Delta^2\right) u_c = \left(u_{ne} + u_{nw} + u_{se} + u_{sw}\right). \qquad \text{(FD2-5X)} \tag{6}$$

Here u_{ne}, u_{nw}, u_{sw} and u_{se} represent the north-eastern, north-western, south-western and south-eastern corner points to u_c. The weighted (four to one ratio) average of Eq. (5) and Eq. (6) leads the following nine-point FD stencil:

$$u_c = \frac{(2/3)\left(u_r + u_u + u_l + u_d\right) + (1/6)\left(u_{ne} + u_{nw} + u_{sw} + u_{se}\right)}{(10/3 - k^2\Delta^2)}. \qquad \text{(FD2-9)} \tag{7}$$

Eq. 7 (FD2-9) uses a 9-point stencil. As we expected, it reduces the numerical spatial dispersion. However, it does very little (see Section 4.2) for improving the temporal dispersion. As a result, most existing FD-FD applications adopt the FD2-5 formulation.

Currently, sixth-order accurate compact 9-point FD methods [15–17] are the most advanced FD formulations for the 2-D inhomogeneous Helmholtz equation given below:

$$\begin{aligned} \left[\Delta + k^2\right] u(z,x) &= f(z,x), \\ \Delta = \nabla_t^2 &= \frac{\partial^2}{\partial z^2} + \frac{\partial^2}{\partial x^2}. \end{aligned} \tag{8}$$

The source term $f(z,x)$ is a given continuous 2-D function. For numerical simulation of passive optical waveguide devices we can remove this term with the assumption $f(z,x) = 0$. Due to symmetry in 2D FD-FD geometry, the central point is related to two quantities, namely the sum of all side point values (denoted by $D_1 = u_r + u_u + u_l + u_d$) and the sum of all corner point values (denoted by $D_2 = u_{ne}+u_{nw}+u_{se}+u_{sw}$.) With these notations, we list the 4th-order, 9-point FD-FD stencil [Eq. (27) Ref. [15],] below:

$$\begin{aligned} &A_0 u_c + A_s D_1 + A_c D_2 = 0. \\ &A_0 = -\frac{10}{3} + k^2\Delta^2\left(1 - \frac{k^2\Delta^2}{12}\right), \quad A_s = \frac{2}{3}, \quad A_c = \frac{1}{6}. \qquad \text{(FD4-9)} \end{aligned} \tag{9}$$

Similarly we list the 6th-order, 9-point FD-FD stencil [Eq. (28)

Ref. [16],] below:

$$d_{20}u_c + d_{21}D_1 + d_{20}D_2 = 0.$$
$$d_{20} = -\frac{10}{3} + k^2\Delta^2\left(\frac{46}{45} - \frac{k^2\Delta^2}{12} + \frac{k^4\Delta^4}{360}\right), \qquad \text{(FD6-9)} \tag{10}$$
$$d_{21} = \frac{2}{3} - \frac{k^2\Delta^2}{90}, \quad d_{22} = \frac{1}{6} + \frac{k^2\Delta^2}{180}.$$

As we can see from References [15, 16], these high-order FD-FD schemes of Eq. (9) and Eq. (10) produce similar matches to the published analytical solution example. Numerical experiments of the FD6-9 stencil with sampling densities of three to four points per wavelength are able to produce accurate results. These methods achieve a low level of sampling which is very close to the theoretical Nyquist-Shannon spatial sampling limit of two points per wavelength.

3. THE THEORY OF CONNECTED LOCAL FIELDS (CLF)

It took more than a decade to develop the FD4-9 stencil since the formulation of the FD2-9 scheme and subsequently eight years to progress to the FD6-9 formulation. The immediate question is whether we can improve on the FD6-9 scheme for the Helmholtz equation. If we use additional information, namely the analytical solution, of the Helmholtz equation the answer to the question is yes. We recently discovered and published [21] a formula based on connecting square patches of local fields. It is structurally equivalent to the nine-point FD-FD coefficients and it possesses superior numerical properties in providing very low temporal and spatial dispersions. In following text, we will derive this new nine-point formulation with Fourier-Bessel series expansion (FBSE) of a local field defined on a square FD patch shown in Fig. 1.

3.1. 1D Homogeneous Case

Although there are many methods for obtaining solutions of the Helmholtz equation in 1-D homogeneous cases, it is helpful to derive the method of connected local fields (CLF) for this straightforward case. Note that it is not necessary for the spacing between adjacent points to be equal the theory of CLF under 1-D case. However, equal spacing in both directions is required by the theory of CLF for 2-D and 3-D cases. In 1D, we seek the local field representation $u^{(0)}(z)$ which is bounded between u_{-1} and u_1

$$u_{-1} = u(-\Delta z), \quad u_0 = u(0), \quad u_1 = u(\Delta z) \tag{11}$$

This local field can be completely expressed in terms of u_{-1} and u_1 when the frequency ω, material index n, wave speed c and hence the wavenumber $k = n\omega/c$, are known. We have:

$$u^{(0)}(z) = u_{-1}\frac{\sin k(\Delta z - z)}{\sin(2k\Delta z)} + u_1\frac{\sin k(z + \Delta z)}{\sin(2k\Delta z)}. \quad -\Delta z \le z \le \Delta z \quad (12)$$

The local field $u^{(0)}(z)$ is written as weighted sum of the two "shifted normalized sine" functions which are, in most cases when $\cos(k\Delta z)$ is not zero, two independent solutions of the 1-D Helmholtz equation. In this form, we can easily derive the FD-like coefficients for the centered point u_0. We have:

$$u_0 = \frac{1}{2\cos(k\Delta z)}u_{-1} + \frac{1}{2\cos(k\Delta z)}u_1. \quad (13)$$

Let us compare Eq. (13) with the FD approximation of the 1-D Helmholtz equation of Eq. (3). We see Eq. (3) can be obtained by replacing the two cosine functions in Eq. (13) by the first two terms of the Taylor series. The standard FD2-3 of Eq. (3) of is only an approximation to the 1-D Helmholtz equation, while the LFE formulation Eq. (13) is an exact solution to 1-D Helmholtz equation. The exact local field solution $u^{(0)}(z)$ is connected to its two neighboring local fields $u^{(-1)}(z)$ and $u^{(1)}(z)$ as $u^{(1)}(z)$ is connected to $u^{(0)}(z)$ and $u^{(2)}(z)$. These local fields are algebraically connected in exactly in the same way like the discrete points $\ldots, u_{-1}, u_0, u_1, \ldots$ are connected by the respective FD-FD scheme. Hence "connected local fields" is the name we choose to describe this proposed method of solving the Helmholtz equation.

3.2. The Simple 2D LFE-5 Formulation

We derive the simple 2D LFE formulation which will lead to an improved five-point FD-FD stencil. In the 2-D theory of CLF we assume that 2-D points are equally spaced in x and z such that $\Delta x = \Delta z = \Delta$. These four points are connected by a circle with a radius $\rho = \sqrt{2}\Delta$. The question is how to better express the field inside this circle in terms of field solutions at u_r, u_u, u_l and u_d. As illustrated in Fig. 2, we expand the local field $u^{(0,0)}(\rho, \varphi)$ in the polar coordinate system with u_c as its center, using all terms up to the second-order Fourier-Bessel series as

$$\begin{aligned} u^{(0,0)}(\rho, \phi) \;\approx\; & a_0 J_0(k\rho) + a_1 J_1(k\rho)\cos\phi + b_1 J_1(k\rho)\sin\phi \\ & + a_2 J_2(k\rho)\cos 2\phi + b_2 J_2(k\rho)\sin 2\phi \end{aligned} \quad (14)$$

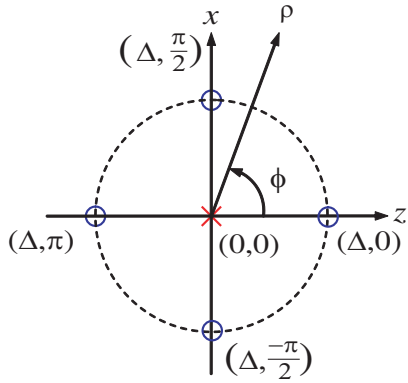

Figure 2. The four side points of u_c shown in a polar coordinate system.

Next we evaluate Eq. (14) at all four side points and we obtain the following equation that relates local field coefficients to EM field on the four side points:

$$\begin{bmatrix} J_0(k\Delta) & J_1(k\Delta) & 0 & J_2(k\Delta) \\ J_0(k\Delta) & 0 & J_1(k\Delta) & -J_2(k\Delta) \\ J_0(k\Delta) & -J_1(k\Delta) & 0 & J_2(k\Delta) \\ J_0(k\Delta) & 0 & -J_1(k\Delta) & -J_2(k\Delta) \end{bmatrix} \begin{bmatrix} a_0 \\ a_1 \\ b_1 \\ a_2 \end{bmatrix} = \begin{bmatrix} u_r \\ u_u \\ u_l \\ u_d \end{bmatrix}. \quad (15)$$

Note that the last Fourier-Bessel coefficient b_2 does not contribute to a new row in Eq. (15) due to $\sin 2\phi$ vanishing at those four polar angles. The inversion formula for the above equation can be readily obtained by noting that the four columns in the matrix of Eq. (15) are orthogonal to each other. Given that the inverse of an orthonormal matrix is simply its transposition, after column scaling and normalization, we obtain an exact inversion formula to Eq. (15). Thus, we have:

$$\begin{bmatrix} a_0 \\ a_1 \\ b_1 \\ a_2 \end{bmatrix} = \begin{bmatrix} \frac{c_0}{4} & \frac{c_0}{4} & \frac{c_0}{4} & \frac{c_0}{4} \\ \frac{c_1}{2} & 0 & -\frac{c_1}{2} & 0 \\ 0 & \frac{c_1}{2} & 0 & -\frac{c_1}{2} \\ \frac{c_2}{4} & -\frac{c_2}{4} & \frac{c_2}{4} & -\frac{c_2}{4} \end{bmatrix} \begin{bmatrix} u_r \\ u_u \\ u_l \\ u_d \end{bmatrix}, \quad (16)$$

$$c_0 = \frac{1}{J_0(k\Delta)}, \quad c_1 = \frac{1}{J_1(k\Delta)}, \quad c_2 = \frac{1}{J_2(k\Delta)}.$$

Eq. (16) provides an analytical expression for Fourier-Bessel coefficients a_0, a_1, b_1, a_2 of a local field $u^{(0,0)}(\rho, \phi)$ in terms of four field entries located on the side points. Furthermore we can solve for u_0 in terms of its immediate neighbors by noting that the zero-order coefficient a_0 is

the only term in Eq. (14) that does not vanish at the origin. Combing Eq. (14) and Eq. (16), we obtain the following discretized version of the Helmholtz equation.

$$u_c = a_0 = \frac{u_r + u_u + u_l + u_d}{4J_0(k\Delta)}. \qquad \text{(LFE-5)} \tag{17}$$

Since Eq. (17) is the structural equivalent to the standard FD-FD equation, all the existing FD-FD methods for handling regions near the interfaces, inhomogeneity, ABC, TBC and the matrix solver, etc. can be used with minor modifications to improve the local accuracy. Due to its improved dispersion characteristics in a homogeneous medium Eq. (17) can be used to reduce memory and CPU resource requirements in the FD-FD computation process. It is interesting to note that Eq. (17) can also be derived under the standard 5-point FD-FD formulation by minimizing the residual phase error of plane wave solution [22].

3.3. The Full 2D LFE-9 Formulation

The simple 2D LFE-5, Eq. (17) is derived from a Fourier-Bessel series expansion of the EM field in a circular patch enclosing five FD points. To obtain the full 2D LFE-9 formulation a larger square patch is needed. Four additional corner points are enclosed in this square local field. This field is expressed as:

$$u^{(0,0)}(\rho,\phi) \approx \sum_{n=0}^{4} a_n J_n(k\rho)\cos\phi + \sum_{n=1}^{3} b_n J_n(k\rho)\sin\phi. \tag{18}$$

Note that b_4 is not included in Eq. (18) as b_2 is not included in Eq. (15). Evaluating the above equation for the eight points on the square we have:

$$\begin{bmatrix}
J_0^s & J_1^s & 0 & J_2^s & 0 & J_3^s & 0 & J_4^s \\
J_0^s & 0 & J_1^s & -J_2^s & 0 & 0 & -J_3^s & J_4^s \\
J_0^s & -J_1^s & 0 & J_2^s & 0 & -J_3^s & 0 & J_4^s \\
J_0^s & 0 & -J_1^s & -J_2^s & 0 & 0 & J_3^s & J_4^s \\
J_0^m & \frac{J_1^m}{\sqrt{2}} & \frac{J_1^m}{\sqrt{2}} & 0 & J_2^m & \frac{-J_3^m}{\sqrt{2}} & \frac{J_3^m}{\sqrt{2}} & -J_4^m \\
J_0^m & \frac{-J_1^m}{\sqrt{2}} & \frac{J_1^m}{\sqrt{2}} & 0 & -J_2^m & \frac{J_3^m}{\sqrt{2}} & \frac{J_3^m}{\sqrt{2}} & -J_4^m \\
J_0^m & \frac{-J_1^m}{\sqrt{2}} & \frac{-J_1^m}{\sqrt{2}} & 0 & J_2^m & \frac{J_3^m}{\sqrt{2}} & \frac{-J_3^m}{\sqrt{2}} & -J_4^m \\
J_0^m & \frac{J_1^m}{\sqrt{2}} & \frac{-J_1^m}{\sqrt{2}} & 0 & -J_2^m & \frac{-J_3^m}{\sqrt{2}} & \frac{-J_3^m}{\sqrt{2}} & -J_4^m
\end{bmatrix}
\begin{bmatrix} a_0 \\ a_1 \\ b_1 \\ a_2 \\ b_2 \\ a_3 \\ b_3 \\ a_4 \end{bmatrix}
=
\begin{bmatrix} u_r \\ u_u \\ u_l \\ u_d \\ u_{ne} \\ u_{nw} \\ u_{sw} \\ u_{se} \end{bmatrix}, \tag{19}$$

$$J_n^s = J_n(k\Delta), \quad J_n^m = J_n(\sqrt{2}k\Delta), \quad n = 0,1,2,3,4.$$

To obtain the FD-like, LFE-9 stencil, we need to find the solution of a_0. If a_0 is all we need; we can reduce the complexity of the 8×8 matrix in Eq. (19) to a mere 2×2 matrix equation. The symmetry condition demands the LFE-9 stencil follow the same form, i.e., $A_0 u_c + A_s D_1 + A_c D_2 = 0$ as does every existing FDx-9 stencil. By summing rows 1–4 in Eq. (19) as the first equation and summing rows 5–8 as the second equation we have the following reduced matrix equation:

$$4 \cdot \begin{bmatrix} J_0^s & J_4^s \\ J_0^m & -J_4^m \end{bmatrix} \begin{bmatrix} a_0 \\ a_4 \end{bmatrix} = \begin{bmatrix} D_1 \\ D_2 \end{bmatrix}. \tag{20}$$

We note that matrix elements in columns 2 to 7 are all zero in the collapsed matrix row group of Eq. (19). Hence, the other six unknowns of Eq. (19) do not contribute to Eq. (20). The analytic solution of Eq. (20) is simply as follows:

$$\begin{bmatrix} a_0 \\ a_4 \end{bmatrix} = \frac{1}{4\left(J_0^s J_4^m + J_0^m J_4^s\right)} \begin{bmatrix} J_4^m & J_4^s \\ J_0^m & -J_0^s \end{bmatrix} \begin{bmatrix} D_1 \\ D_2 \end{bmatrix}. \tag{21}$$

The solution of a_0 leads to the following LFE-9 equation:

$$u_c = \frac{1}{4} \frac{\begin{array}{c} J_4\left(\sqrt{2}k\Delta\right) \cdot (u_r + u_u + u_l + u_d) \\ +J_4\left(k\Delta\right) \cdot (u_{ne} + u_{nw} + u_{se} + u_{sw}) \end{array}}{J_0\left(k\Delta\right) \cdot J_4\left(\sqrt{2}k\Delta\right) + J_0\left(\sqrt{2}k\Delta\right) \cdot J_4\left(k\Delta\right)}. \qquad \text{(LFE-9)} \tag{22}$$

This recently published LFE-9 formulae is structurally equivalent to the nine-point FD-FD stencils such as FD2-9 (Eq. (7)), FD4-9 (Eq. (9)) and FD6-9 (Eq. (10)). We shall prove in future paper that high-order compact stencils like Eqs. (7), (9), and (10) can be derived from LFE-9 formulation.

3.4. The LFE-9 Reconstruction Formulae

One of the unique features of our proposed theory of connected local field is that within each square patch, there is an analytical expression for the local field in terms of the truncated local Fourier-Bessel series. Furthermore, Eq. (19) is the link between the eight-term Fourier-Bessel series and the eight EM field values sampled on the sides and corners. As a result, the local field (inside the square patch) can be reconstructed/interpolated in terms of said eight points. For other FD-FD methods, an arbitrary field must be interpolated by some two-dimensional interpolation methods such as the bilinear or bicubic spline interpolation methods [23, 24]. Let us derive the closed-form expression for the LFE-9 reconstruction formulae. At first sight, a symbolic/analytical inversion of an 8×8 matrix is a daunting task

if not impossible. Fortunately by exploiting the built-in symmetry structure of this problem, it can be completed. We see that there are two point groups in Eq. (19), namely the side points and the corner points. The members in the plus (side) group $\mathbf{u}_+ = [u_r, u_u, u_l, u_d]^T$ are distanced Δ away from the central point whereas the members in the cross (corner) group $\mathbf{u}_\times = [u_{ne}, u_{nw}, u_{sw}, u_{se}]^T$ are located $\sqrt{2}\Delta$ away from the referenced point u_c. In terms of these two vectors we may rewrite Eq. (19) into the following compact 2×2 matrix:

$$\begin{bmatrix} \mathbf{Q}_{11} & \mathbf{Q}_{12} \\ \mathbf{Q}_{21} & \mathbf{Q}_{22} \end{bmatrix} \begin{bmatrix} \mathbf{c}_L \\ \mathbf{c}_H \end{bmatrix} = \begin{bmatrix} \mathbf{u}_+ \\ \mathbf{u}_\times \end{bmatrix}, \tag{23}$$

where $\mathbf{c}_L = [a_0, a_1, b_1, a_2]$ is the low FB coefficient vector and $\mathbf{c}_H = [b_2, a_3, b_3, a_4]^T$ is the high FB coefficient vector. The inversion formula for the above equation can be obtained by noting that the columns in $\mathbf{Q}_{11}$ and $\mathbf{Q}_{22}$ of Eq. (23) are orthogonal to each other therefore, the exact inverse of $\mathbf{Q}_{11}$ and $\mathbf{Q}_{22}$ can be obtained To solve for $\mathbf{c}_L$ we first use the second Eq. (23) and express $\mathbf{c}_H$ as

$$\mathbf{c}_H = \left(\mathbf{Q}_{22}^{-1}\right)\left(\mathbf{u}_\times - \mathbf{Q}_{21}\mathbf{c}_L\right). \tag{24}$$

Thus we have

$$\mathbf{c}_L = \left(\mathbf{Q}_{11} - \mathbf{Q}_{12}\mathbf{Q}_{22}\mathbf{Q}_{21}\right)^{-1}\left(\mathbf{u}_+ - \mathbf{Q}_{12}\mathbf{Q}_{22}\mathbf{u}_\times\right). \tag{25}$$

In a similar way we obtain

$$\mathbf{c}_H = \left(\mathbf{Q}_{22} - \mathbf{Q}_{21}\mathbf{Q}_{11}^{-1}\mathbf{Q}_{12}\right)^{-1}\left(\mathbf{u}_\times - \mathbf{Q}_{21}\mathbf{Q}_{11}^{-1}\mathbf{u}_+\right). \tag{26}$$

After a few algebraic steps, we have the analytic formulae for FB coefficients. They are, as expressed in four groups listed below:

$$\begin{aligned} a_0 &= \frac{J_4^m\left(u_r + u_u + u_l + u_d\right) + J_4^s\left(u_{ne} + u_{nw} + u_{sw} + u_{se}\right)}{4\left(J_0^s J_4^m + J_0^m J_4^s\right)}, \\ a_4 &= \frac{J_0^m\left(u_r + u_u + u_l + u_d\right) - J_0^s\left(u_{ne} + u_{nw} + u_{sw} + u_{se}\right)}{4\left(J_0^s J_4^m + J_0^m J_4^s\right)}. \end{aligned} \tag{27}$$

$$\begin{aligned} a_1 &= \frac{\sqrt{2}J_3^m\left(u_r - u_l\right) + J_3^s\left(u_{ne} - u_{nw} - u_{sw} + u_{se}\right)}{2\sqrt{2}\left(J_1^s J_3^m + J_1^m J_3^s\right)}, \\ b_1 &= \frac{\sqrt{2}\,J_3^m\left(u_u - u_d\right) + J_3^s\left(u_{ne} + u_{nw} - u_{sw} - u_{se}\right)}{2\sqrt{2}\left(J_1^s J_3^m + J_1^m J_3^s\right)}. \end{aligned} \tag{28}$$

$$\begin{aligned} a_2 &= \frac{\left(u_r - u_u + u_l - u_d\right)}{4J_2^s}, \\ b_2 &= \frac{\left(u_{ne} - u_{nw} + u_{sw} - u_{se}\right)}{4J_2^m}. \end{aligned} \tag{29}$$

$$
\begin{aligned}
a_3 &= \frac{\sqrt{2}J_1^m\left(u_r - u_l\right) + J_1^s\left(-u_{ne} + u_{nw} + u_{sw} - u_{se}\right)}{2\sqrt{2}\left(J_1^s J_3^m + J_1^m J_3^s\right)}, \\
b_3 &= \frac{\sqrt{2}J_1^m\left(-u_u + u_d\right) + J_1^s\left(u_{ne} + u_{nw} - u_{sw} - u_{se}\right)}{2\sqrt{2}\left(J_1^s J_3^m + J_1^m J_3^s\right)}.
\end{aligned} \tag{30}
$$

Equation (19) and Eqs. (27)–(30) are all we need for the reconstruction of a 2D local field In the next section we will examine and compare numerical dispersion properties of all these FD-FD stencils.

4. DISPERSION CHARACTERISTICS

The theoretical phase velocity of a plane wave propagating in an ideal linear non-dispersive medium is constant independent of the frequency and the direction of propagation. When the Helmholtz equation is solved by numerical methods such as the FD-FD method or our CLF method the equivalent phase velocity of a plane wave depends on the frequency as well as the direction of propagation. Numerical dispersion is the difference between these two phase velocities. It is good to know that for an infinite homogeneous media, at any given frequency, there exists infinite number of plane wave solutions to both the 2-D Helmholtz partial differential equation and the discretized Helmholtz FD equation. The analytical plane wave solution is given by:

$$u\left(z,x\right) = e^{-j\mathbf{k}\cdot\rho}, \tag{31}$$

where $\boldsymbol{\rho} = (z,x)$ and the vector symbol $\mathbf{k} = (k_z,k_x) = k\left(\cos\theta,\sin\theta\right)$ denotes the vectorial analytic wavenumber of the plane wave propagating in the θ direction. In an infinite homogeneous medium, every point has an identical FD equation with its neighboring points. There is no need to solve for the infinitely huge matrix equation in a source-free medium while we look for a plane wave solution. Thus, given a FD-like method, we look for a discretized solution of the following form:

$$
\begin{aligned}
&u\left(z_i,x_j\right) = \exp\left(-j\boldsymbol{\kappa}\cdot\boldsymbol{\rho}_{i,j}\right), \\
&\boldsymbol{\rho}_{i,j} = \left(z_i,x_j\right) \quad z_i = i\Delta, \quad x_j = j\Delta.
\end{aligned} \tag{32}
$$

Here the symbol (kappa) $\boldsymbol{\kappa} = (\kappa_z,\kappa_x) = \kappa\left(\cos\theta,\sin\theta\right)$ denotes the vectorial numerical wavenumber of the plane wave propagating in the θ direction. The field on the circle of radius ρ will be:

$$u\left(\rho\cos\phi,\rho\sin\phi\right) = e^{j\kappa\rho\cos(\phi-\theta)}. \tag{33}$$

Evaluating this equation at u_r, u_u, u_l, u_d and u_c we have:

$$\begin{aligned} u_r &= e^{j\kappa\Delta\cos\theta}, \quad & u_u &= e^{j\kappa\Delta\sin\theta}, \\ u_l &= e^{-j\kappa\Delta\cos\theta}, \quad & u_d &= e^{-j\kappa\Delta\sin\theta}, \\ u_c &= 1. \end{aligned} \tag{34}$$

Similarly, evaluate this equation at u_{ne}, u_{nw}, u_{se} and u_{sw} we have:

$$\begin{aligned} u_{ne} &= e^{j\sqrt{2}\kappa\Delta\cos(\theta-\pi/4)}, \quad & u_{nw} &= e^{j\sqrt{2}\kappa\Delta\sin(\theta-\pi/4)}, \\ u_{sw} &= e^{-j\sqrt{2}\kappa\Delta\cos(\theta-\pi/4)}, \quad & u_{se} &= e^{-j\sqrt{2}\kappa\Delta\sin(\theta-\pi/4)}. \end{aligned} \tag{35}$$

Thus,

$$D_1 = u_r + u_u + u_l + u_d = 2\left[\cos\left(\kappa\Delta\cos\theta\right) + \cos\left(\kappa\Delta\sin\theta\right)\right]. \tag{36}$$

Similarly we have

$$\begin{aligned} D_2 \;=\; u_{ne} + u_{nw} + u_{se} + u_{sw} &= 2\cos\left(\sqrt{2}\kappa\Delta\cos\left(\theta - \frac{\pi}{4}\right)\right) \\ &+2\cos\left(\sqrt{2}\kappa\Delta\sin\left(\theta - \frac{\pi}{4}\right)\right). \end{aligned} \tag{37}$$

4.1. Numerical Dispersion Characteristics of the FD2-5 Case

To obtain the numerical dispersion relation for the standard five-point FD-FD scheme we substitute Eq. (36) into Eq. (4) and we have

$$4 - k^2\Delta^2 = 2\left[\cos\left(\kappa\Delta\cos\theta\right) + \cos\left(\kappa\Delta\sin\theta\right)\right]. \qquad \text{(FD2-5)} \tag{38}$$

Note that $\kappa = \sqrt{\kappa_x^2 + \kappa_z^2}$ and that $k \neq \kappa$. This nonlinear equation gives the exact relation between $\boldsymbol{\kappa}$ and $\mathbf{k}$, the numerical and the analytical wavenumber of the plane wave propagating in an infinite homogeneous medium. In other words, the numerical $\boldsymbol{\kappa}$ is an implicit function of $\mathbf{k}$ which is function of frequency and direction of propagation. An alternate form for Eq. (34) is given by [25]

$$k = \kappa\sqrt{\cos^2\theta\left[\frac{\sin\left(\frac{\kappa\Delta\cos\theta}{2}\right)}{\left(\frac{\kappa\Delta\cos\theta}{2}\right)}\right]^2 + \sin^2\theta\left[\frac{\sin\left(\frac{\kappa\Delta\sin\theta}{2}\right)}{\left(\frac{\kappa\Delta\sin\theta}{2}\right)}\right]^2}. \tag{39}$$

It is easy to see that as $\Delta \to 0$ we have the linear isotropic dispersion relation $k = \kappa$.

4.2. Numerical Dispersion Characteristics of the FD2-9 Case

Substituting Eqs. (36), (37) into Eq. (7), we have the numerical dispersion relation for FD2-9 stencil:

$$\begin{aligned} 10 - 3k^2\Delta^2 = 4\cos(\kappa\Delta\cos\theta) + 4\cos(\kappa\Delta\sin\theta) + \cos\left(\sqrt{2}\kappa\Delta\cos\left(\theta - \frac{\pi}{4}\right)\right) \\ + \cos\left(\sqrt{2}\kappa\Delta\sin\left(\theta - \frac{\pi}{4}\right)\right). \qquad \text{(FD2-9)} \end{aligned} \tag{40}$$

The additional terms in Eq. (40) improves the "isotropicness" of the FD2-9 formulation over FD2-5.

4.3. Numerical Dispersion Characteristics of LFE-5 Case

To obtain the numerical dispersion relation for the 2D FB-LFE formulation (which will be denoted as LFE-5), we substitute Eq. (17) into Eq. (36) and we have

$$2J_0(k\Delta) = \cos(\kappa\Delta\cos\theta) + \cos(\kappa\Delta\sin\theta). \qquad \text{(LFE-5)} \qquad (41)$$

4.4. Numerical Dispersion Characteristics of the LFE-9 Case

To obtain the numerical dispersion relation for the 2D LFE-9 formulation we substitute Eq. (19) into Eq. (24) and we have

$$\begin{aligned} &2\left[J_0\left(\sqrt{2}\,k\Delta\right)\cdot J_4(k\Delta) + J_0(k\Delta)\cdot J_4\left(\sqrt{2}\,k\Delta\right)\right] \\ &= J_4\left(\sqrt{2}\,k\Delta\right)\cdot\left[\cos(\kappa\Delta\cos\theta) + \cos(\kappa\Delta\sin\theta)\right] \\ &\quad + J_4(k\Delta)\cdot\left(\cos\left(\sqrt{2}\kappa\Delta\cos\left(\theta-\frac{\pi}{4}\right)\right) + \cos\left(\sqrt{2}\kappa\Delta\sin\left(\theta-\frac{\pi}{4}\right)\right)\right). \end{aligned}$$

(LFE-9) (42)

4.5. Low Frequency Dispersion Analysis for FD2-5, FD2-9 and LFE-5 Formulae

To better understand the order of errors in FD2-5 and FD2-9 at low frequency, we apply the following Taylor's expansion to the right hand sides of Eqs. (38) and (40):

$$\cos(z) = \sum_{n=0}^{\infty} \frac{(-1)^n}{(2n)!}\, z^{2n} \approx 1 - \frac{1}{2}z^2 + \frac{1}{24}z^4 - \frac{1}{720}z^6. \qquad (43)$$

To simplify the expression, we first define the normalized analytical wavenumber V and the corresponding normalized numerical wavenumber B as

$$V \triangleq k\Delta, \quad B \triangleq \kappa\,\Delta. \qquad (44)$$

We also need the following side calculations for the right hand size of Eqs. (38), (40), and (41):

$$\begin{aligned}
&\cos(B\cos\theta)+\cos(B\sin\theta)\\
&\approx\left(1-\frac{B^2\cos^2\theta}{2}+\frac{B^4\cos^4\theta}{24}-\frac{B^6\cos^6\theta}{720}\right)\\
&\quad+\left(1-\frac{B^2\sin^2\theta}{2}+\frac{B^4\sin^4\theta}{24}-\frac{B^6\sin^6\theta}{720}\right),\\
&=2-\frac{1}{2}B^2+\frac{B^4}{96}(3+\cos 4\theta)-\frac{B^6}{5760}(5+3\cos 4\theta),
\end{aligned}\tag{45}$$

and

$$\begin{aligned}
&\cos(B(\sin\theta+\cos\theta))+\cos(B(\sin\theta-\cos\theta))\\
&\approx\left(1-\frac{1}{2}B^2(\sin\theta+\cos\theta)^2+\frac{B^4}{24}(\sin\theta+\cos\theta)^4-\frac{B^6}{720}(\sin\theta+\cos\theta)^6\right),\\
&+\left(1-\frac{1}{2}B^2(\sin\theta-\cos\theta)^2+\frac{B^4}{24}(\sin\theta-\cos\theta)^4-\frac{B^6}{720}(\sin\theta-\cos\theta)^6\right),\\
&=2-B^2+\frac{B^4}{12}\left(\sin^4\theta+\cos^4\theta+6\sin^2\theta\cos^2\theta\right)-\frac{B^6}{720}(5-3\cos 4\theta),\\
&=2-B^2+\frac{B^4}{24}(3-\cos 4\theta)-\frac{B^6}{720}(5-3\cos 4\theta).
\end{aligned}\tag{46}$$

Now we may express the dispersion error for FD2-5 and FD2-9 as

$$\begin{aligned}
&4-V^2=2\cos(B\cos\theta)+2\cos(B\sin\theta),\\
&V^2=B^2-\frac{B^4}{48}(3+\cos 4\theta)+\frac{B^6}{2880}(5+3\cos 4\theta),\qquad\text{(FD2-5)}
\end{aligned}\tag{47}$$

and:

$$\begin{aligned}
10-3V^2&=4(\cos(B\cos\theta)+\cos(B\sin\theta)),\\
&\quad+\cos(B(\sin\theta+\cos\theta))+\cos(B(\sin\theta-\cos\theta)),\\
&=8-2B^2+\frac{B^4}{24}(3+\cos 4\theta)-\frac{B^6}{1440}(5+3\cos 4\theta),\\
&\quad+2-B^2+\frac{B^4}{24}(3-\cos 4\theta)-\frac{B^6}{720}(5-3\cos 4\theta),\quad\text{(FD2-9)}\\
V^2&=B^2-\frac{B^4}{12}+\frac{B^6}{1440}(5-\cos 4\theta).
\end{aligned}\tag{48}$$

For the dispersion error of LFE-5 case, we use the following Taylor's expansion of the Bessel function in Eq. (41):

$$J_0(z)=\sum_{n=0}^{\infty}\frac{(-1)^n}{(n!)^2}\left(\frac{z}{2}\right)^{2n}\approx 1-\frac{1}{4}z^2+\frac{1}{64}z^4-\frac{1}{2304}z^6.\tag{49}$$

This would lead to following expression:

$$\begin{aligned} &2J_0(V) = \cos(B\cos\theta) + \cos(B\sin\theta), \\ &V^2 - \frac{V^4}{16} + \frac{V^6}{576} = B^2 - \frac{B^4}{48}(3+\cos 4\theta) + \frac{B^6}{2880}(5+3\cos 4\theta). \quad \text{(LFE-5)} \end{aligned} \tag{50}$$

The above analysis becomes too complicated for the dispersion error of LFE-9 case. We simply leave that to the numerical analysis in Section 5. Here we summarize the $B-V$ relationship at low frequencies when B and V are both less than 1.

$$\begin{aligned} &B^2 = V^2 + \tfrac{B^4}{48}(3+\cos 4\theta), && \text{(4th-degree FD2-5)} \\ &B^2 = V^2 - \tfrac{V^4}{16} + \tfrac{B^4}{48}(3+\cos 4\theta) && \text{(4th-degree LFE-5)} \\ &B^2 = V^2 + \tfrac{B^4}{12}. && \text{(4th-degree FD2-9)} \\ &B^2 = V^2 + \tfrac{B^4}{12} - \tfrac{B^6}{1440}(5-\cos 4\theta). && \text{(6th-degree FD2-9)} \end{aligned} \tag{51}$$

In overall performance, FD2-9 is worse than FD2-5 in temporal dispersion for most plane wave angles except when θ equals to an integer multiple of $\pi/2$. At those incident angles, the phase errors are identical for FD2-5 and FD2-9. However, FD2-9 has a lower order of angular variation than FD2-5. In fact the 4th degree angular dispersion is zero for FD2-9. Another interesting point is that when θ equals to integer multiple of $\pi/8$, the 4th degree numerical dispersion error for LFE-5 is zero; i.e., at low frequencies B and V are equal up to the 4th power. This implies all existing 2nd-order accurate FD-FD programs benefit from a simple replacement of the FD coefficients with those of LFE-5.

5. NUMERICAL DISPERSION STUDY OF LEF-9 FORMULATION

LFE-9 dispersion characteristics are much more complex than those in the FD2-5, FD2-9 and LFE-5 cases. Analytical dispersion error analysis for the LFE-9 formula will have to wait for further developments. In this section, we will numerically evaluate and compare these four cases to demonstrate the advantages of the LFE-9 formulation. Comparisons of the LFE-9 performance with compact high-order 9 point FD-FD stencils of FD4-9 and FD6-9 will be detailed in our future works.

5.1. V Versus B Curves

In waveguide analysis, we study $k-\beta$ curves. The slope of the line connecting a point on the $k-\beta$ to the origin is the ratio of phase

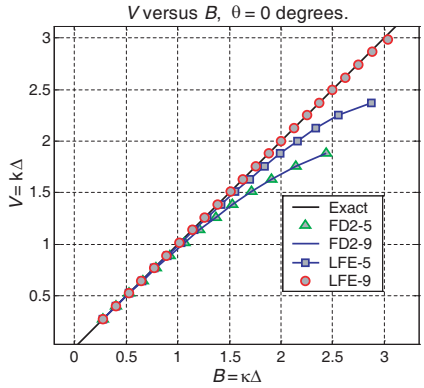

Figure 3. V versus B for FD2-5, FD2-9, LFE-5 and LFE-9 formulae. The plane wave incident angle is fixed at $\theta = 0$ degrees. The maximum range of V, the normalized analytic wavenumber, is π.

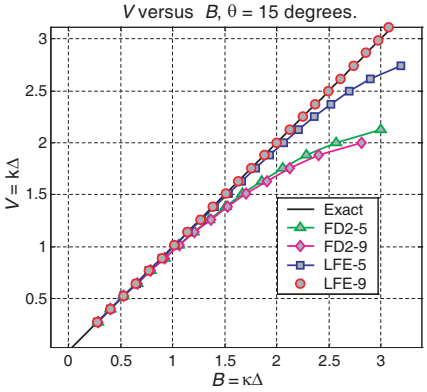

Figure 4. V versus B for FD2-5, FD2-9, LFE-5 and LFE-9 formulae. The plane wave incident angle is fixed at $\theta = 15$ degrees. The maximum range of V, the normalized analytic wavenumber, is π.

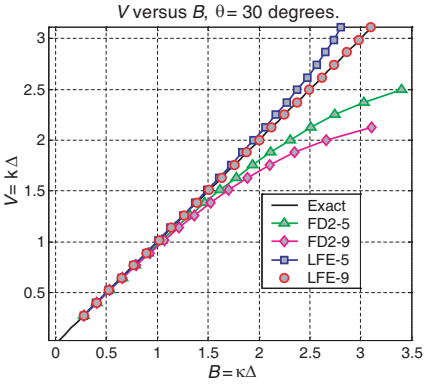

Figure 5. V versus B for FD2-5, FD2-9, LFE-5 and LFE-9 formulae. The plane wave incident angle is fixed at $\theta = 30$ degrees. The maximum range of V, the normalized analytic wavenumber, is π.

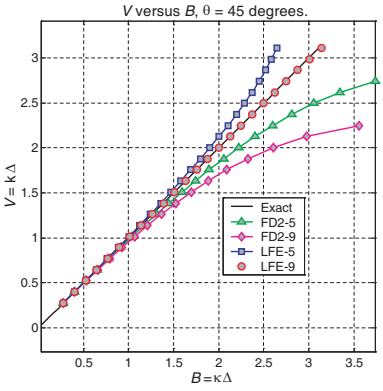

Figure 6. V versus B for FD2-5, FD2-9, LFE-5 and LFE-9 formulae. The plane wave incident angle is fixed at $\theta = 45$ degrees. The maximum range of V, the normalized analytic wavenumber is, π. Note that $B < V$ for LFE-5.

velocity over the speed of light. The tangent of a point on the curve stands for the ratio of the group velocity over speed of light [26, 27]. Here we consider a given FD-FD method with the numerical grid as some special waveguide and we can study its $k - \beta$ characteristics. Using the normalized analytic wavenumber $V = k\Delta$ as our y-axis and normalized numerical wavenumber $B = \kappa\Delta$ as our x-axis. In Figs. 3–6, we plot $K - B$ curves for FD2-5, FD2-9, LFE-5 and LFE-9 formulae with incident angles fixed at 0, 15, 30 and 45 degrees. These dispersion curves are periodic functions with a period of $\pi/4$. They are also even with respect to the $\theta = \pi/8$ axis.

From these figures we see the the LFE-9 curves follow very closely to the exact $V = B$ black curves. In most cases FD2-5 shows better performance than FD2-9 except when they are equal that when the incident angles θ are fixed at some integer multiple of $\pi/2$. We also learn that the normalized numerical wavenumbers B are greater than the normalized analytic wavenumbers V. We note, from Fig. 6, an exception to this rule that $B < V$ on some of the LFE-5 curves.

5.2. Relative Dispersion Errors as Function of Sampling Density

In running FD-FD programs, the user is asked to choose a free simulation parameter, namely, the sampling density. In our paper we label it N_λ where is defined as

$$N_\lambda = \frac{\lambda}{n\Delta} = \frac{\pi}{V}. \tag{52}$$

We usually set $N_\lambda = 20$ in running FD2-5 codes to ensure a less than 1% phase error. Setting N_λ to a high value is very costly. Most computational costs in running 2D FD2-5 codes are the time and computer core memory needed to inverse a huge banded sparse matrix. The theoretical CPU run time is proportional to $(N_\lambda)^4$ while the memory required is proportional to $(N_\lambda)^3$. This is why we are interested in the numerical method that would ask for a smaller N_λ for a given accuracy requirement. In Figs. 7–10, we plot the relative dispersion error ε as function of sampling density for FD2-5, FD2-9, LFE-5 and LFE-9 formulae with incident angles fixed at 0, 15, 21 and 22.5 degrees. The relative phase error ε is defined as

$$\varepsilon = \frac{|V - B|}{V}. \tag{53}$$

From its definition ε can also be interpreted as a relative phase velocity error. The range of N_λ starts from a low $N_\lambda = 2$ to a high $N_\lambda = 50$.

It is interesting to note from Fig. 10 that LFE-5 is more accurate than LFE-9 for plane wave propagating at $\theta = 22.5$ degrees. Its performance degrades immediately when the propagation angle deviates for only a few degrees as seen from Fig. 9. From Figs. 7–10 we can clearly see that LFE-9 curves possess superior numerical properties of being extremely flat except where N_λ close to 2.

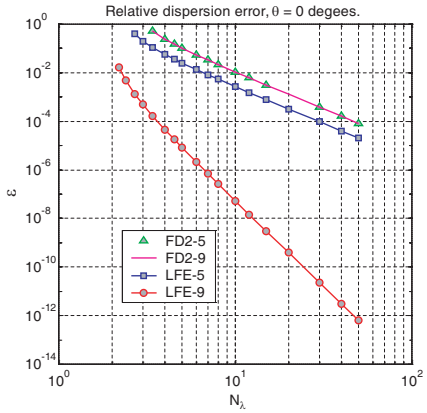

Figure 7. Relative phase dispersion errors for FD2-5, FD2-9, LFE-5 and LFE-9 at $\theta = 0$ degrees.

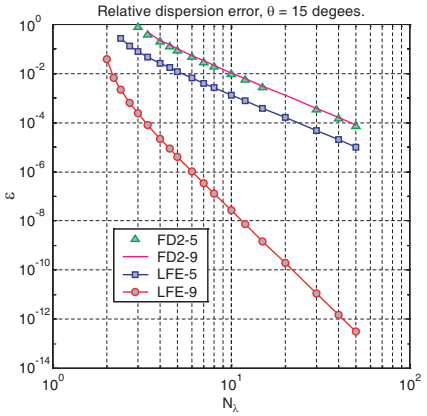

Figure 8. Relative dispersion errors for FD2-5, FD2-9, LFE-5 and LFE-9 at $\theta = 15$ degrees.

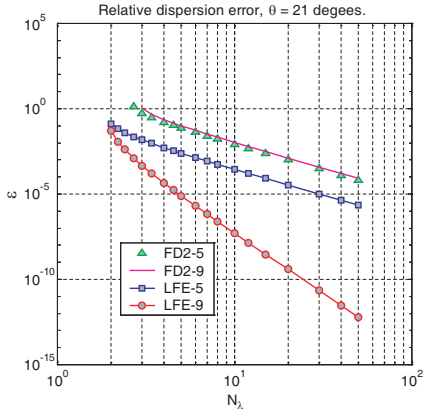

Figure 9. Relative dispersion errors for FD2-5, FD2-9, LFE-5 and LFE-9 at $\theta = 21$ degrees.

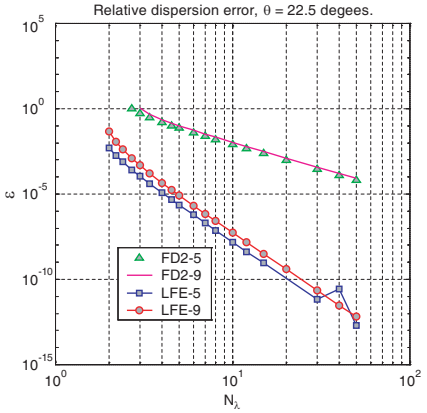

Figure 10. Relative dispersion errors for FD2-5, FD2-9, LFE-5 and LFE-9 at $\theta = 22.5$ degrees.

5.3. Numerical Study of LFE-9 Spatial Dispersion

Finally, in Figs. 11–16 we plot n_B as function of direction for FD2-5, FD2-9, LFE-5 and LFE-9 formulae with a fixed N_λ. The effective index n_B, which is a function of frequency as well as plane wave propagation direction, is defined as:

$$n_B = \frac{B}{V}. \tag{54}$$

We can clearly see from Figs. 11–16 that LFE-9 curves possess superior isotropic properties that the effective numerical index n_B is virtually sitting on top of the unit circle and the differences only become noticeable when $N_\lambda = 2.1$ ($V = 1.5$). In fact, when $V < 1$ ($N_\lambda > \pi$), the relative phase error for LFE-9 which is defined as $\varepsilon_{\text{LFE-9}} = (B_{\text{LFE-9}} - V)/V$, can be shown (detail to be published) to be:

$$\varepsilon_{\text{LFE-9}} = \left[\frac{1.29\left(1 - \frac{11k^2\Delta^2}{100} + \frac{k^4\Delta^4}{225}\right)\cos(8\theta)}{1 - \frac{k^2\Delta^2}{4} + \left(\frac{33-\cos(4\theta)}{1440}\right)k^4\Delta^4}\right]\left(\frac{k\Delta}{10}\right)^6. \tag{55}$$

From reading the slopes of LFE-9 curves in Figs. 6–10, we can verify this low, 6th order phase error of $\varepsilon_{\text{LFE-9}}$ in Eq. (55). Like LFE-5, the relative phase error of LFE-9 does not have a DC term. We note that $\varepsilon_{\text{LFE-9}}$ is a periodic function of θ and in its fundamental period $0 \le \theta \le \pi/4$, the two normalized frequencies B and V are competing with each other that:

$$\begin{cases} B < V, & \dfrac{\pi}{16} \le \theta \le \dfrac{3\pi}{16}, \\ B > V, & \text{otherwise.} \end{cases} \tag{56}$$

6. PRINCIPLES OF CONNECTED LOCAL FIELDS

There are basically two types of methods, analytic and numerical, for solving the inhomogeneous Helmholtz equation in a piece-wise constant medium. Analytic or semi-analytical methods such as coupled transverse-mode integral equation methods [28, 29] and mode-matching methods [30, 31] break the problem into sub-regions whose solutions are made of some linear combinations of exact basis functions These methods focus on matching the tangential fields along the borders where sub-regions meet. They are very powerful but difficult to implement for complex waveguide devices. On the other hand, FD-FD and FD-FE (finite-element) methods [32, 33] are a lot more versatile and can be tailored for complex structures. These methods handle the interface conditions with ease but spend computational resources on

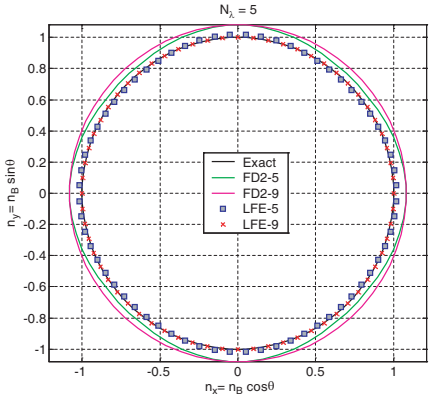

Figure 11. Spatial dispersion for FD2-5, FD2-9, LFE-5 and LFE-9 at $N_\lambda = 5$.

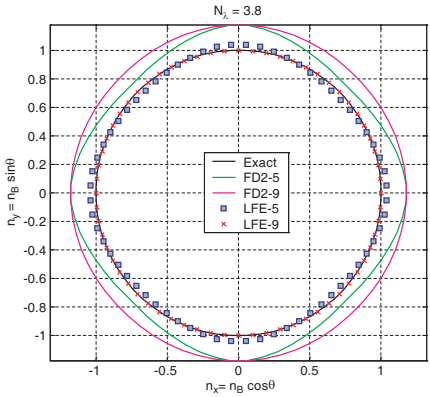

Figure 12. Spatial dispersion for FD2-5, FD2-9, LFE-5 and LFE-9 at $N_\lambda = 3.8$.

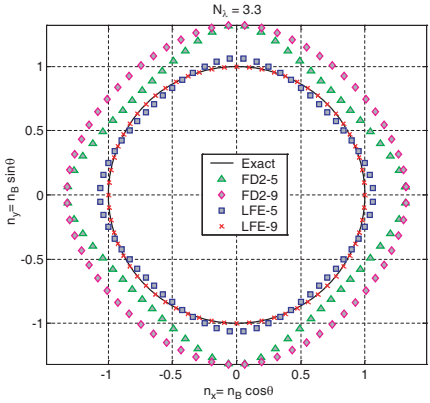

Figure 13. Spatial dispersion for FD2-5, FD2-9, LFE-5 and LFE-9 at $N_\lambda = 3.3$.

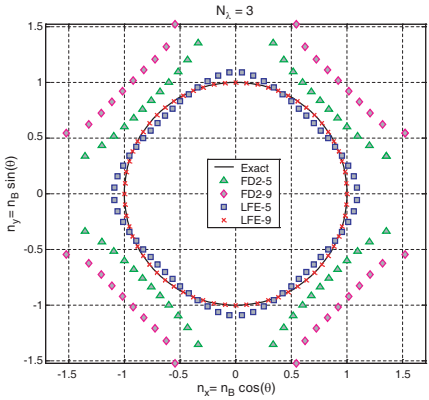

Figure 14. Spatial dispersion for FD2-5, FD2-9, LFE-5 and LFE-9 at $N_\lambda = 3.0$.

solving the Helmholtz equation. The method of connected local fields is the mixture of both types of methods. Like analytical methods, CLF starts with some linear combination of exact "local" basis functions. There is no need to numerically solve for the Helmholtz equation. Unlike the analytical method, CLF does not match tangential fields across material interfaces, since these interface/boundary conditions are handled during the construction of LFE coefficients in every square patch containing two materials or more. In fact, CLF pre-solves many

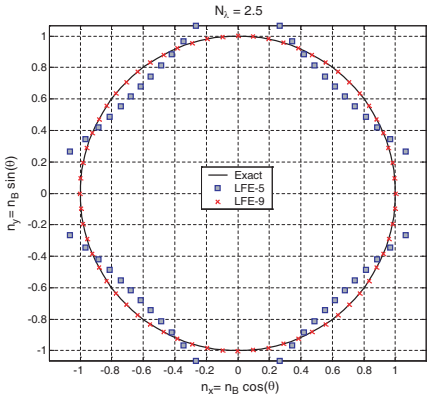

Figure 15. Spatial dispersion for LFE-5 and LFE-9 at $N_\lambda = 2.5$.

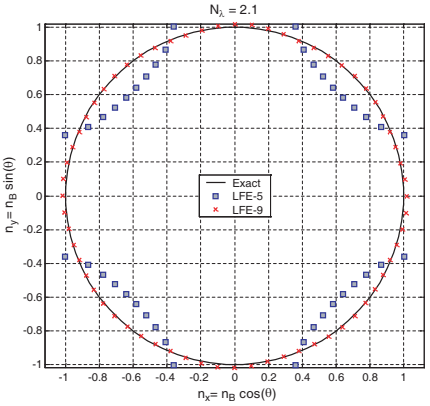

Figure 16. Spatial dispersion for LFE-5 and LFE-9 at $N_\lambda = 2.1$.

small problems analytically and store the results in a library. It then combines the local solutions and forms a matrix equation like the FD-FD method with a compact 9-point stencil.

What is new in the method of connected local fields is that the solution consists of a rectangular array of overlapping patches of local fields. Within each patch there is a centered (reference) point surrounded by eight neighboring points. This squared field is expressed in terms of a truncated Fourier-Bessel series (FBS) of up to the 4th order Bessel function. Since each grid point acts as a reference point for its local field, these patches of unit cells overlap one another very much like cellular phone reception coverage. As a result, each FBS is coupled to all eight neighboring FBSs. Four local fields simultaneously define the field at a given point. For example, in Fig. 1, for a field $u(z, x)$ in the first quadrant $0 < z < \Delta,\ 0 < x < \Delta$, it is defined simultaneous by four local fields centered at $u_c,\ u_r,\ u_{ne}$ and u_u respectively. The virtue of CLF is that every local field exactly satisfies the Helmholtz equation It is only natural to pursue the "equation" governing these FBSs.

At this stage we can set up equations for these FBSs using the point matching principle or by a mode matching method. Such an approach will result in a block tri-diagonal matrix equation for the unknown arrays of FSBs. Since each block will be made of a full 8×8 full matrix, it would not be as computationally efficient as existing methods such those high-order FD schemes FD4-9 and FD6-9. A different approach is to take advantage of the fact that each square patch, the FBS and the eight field values on the square boundary

are equivalent LFE analysis provides the exact link between FBS and bordering points through Eq. (22). Furthermore, each centered point in a given square patch is also a side point or a corner point on eight other neighboring patches. LFE-9 provides a linear equation linking every centered point with its boundary points. Thus, all points on the 2-D grids of the theory of CLF are inter-connected just like a high-order FD-FD method connects its 2D unknowns with a compact nine point stencil.

Once the linear equation for CLF is solved, the entire solutions are made of patches of local fields each capable of an analytic expression reconstruction, by the eight points enclosing the patch. Hence our proposed theory of CLF provides semi-analytical solutions to the 2-D Helmholtz equation as stated in the title of this paper.

7. DISCUSSION

There are many questions waiting to be answered in this new theory of CLF. For example, are the four field representations of one of four sub-domains (with an area of Δ^2) of Fig. 1 identical? If not, how much do they differ from one another? We will try to address this issue in our follow-up paper where we shall study the CLF solution of the 2D Green's function of the Helmholtz equation and its error statistics by comparing it with the exact analytical solution.

7.1. Extension to Inhomogeneous Cases

Although we presented our CLF theory for a homogeneous medium, it can be directly extended to a medium with continuous index variations by assuming a constant index in each square patch. For those inhomogeneous media with step discontinuities, modifications to the LFE coefficients will be required if we want to maintain the same level of accuracy for all local fields. Before we complete building the library of LFE coefficients for these special patches we can always resort to methods using either the simple weighted averaged FD coefficients [4, 6] or other published works for constructing FD-FD coefficients near a junction or curve surfaces [22, 34].

7.2. Extension to 3-D Cases

We are also working on an extension of CLF theory for the 3-D case. In a 3D CLF, the basic patch is a cube. The size of the equivalent FD-FD stencil will be twenty seven. On the boundary of the cube there are a total of 26 points, six on the faces (facets, sides), twelve on the

edges and eight on the vertices (corners). It is however, not an easy task to carry out the 3D LFE extension since between orders zero to four, there are only a total of 25 terms in the truncated series of the spherical harmonics. With the last term, $j_4(kr)P_4^4(\cos\theta)\sin 4\phi$ [26], not contributing to any of these special 26 points on the surface of the cube, we are faced with the problem of setting up 26 equations with only 24 unknowns. We expect the analytical reconstruction formula, if derived, will be too complex to be practically applicable.

8. CONCLUSIONS

The standard second-order accurate FD-FD method requires a more than 10 points per wavelength sampling of the time-harmonic EM wave field. As a result, the FD-FD matrix equation becomes too large for most 3D problems and in many cases for some complex 2D optical waveguide devices. We derive and propose a new compact nine-point FD-FD stencil based on local Fourier-Bessel expansion for the 2-D Helmholtz equation in a homogeneous medium. Our LFE-9 formulation includes an analytic reconstruction equation for the local field in a square patch. We also investigate, in detail, the numerical dispersion characteristics of this LFE-9 equation. Our results show that LFE-9 is capable of reducing the sampling density of a FD-FD simulation to just a little more than two points per wavelength which is Nyquist-Shannon's sampling theorem's theoretical limit.

ACKNOWLEDGMENT

We are grateful for the support of the National Science Council of the Republic of China under the contracts NSC98-2221-E110-012. This work is also supported by the Ministry of Education, Taiwan, under the Aim-for-the-Top University Plan.

REFERENCES

1. Hadley, G. R., "High-accuracy finite-difference equations for dielectric waveguides I: Uniform regions and dielectric interfaces," *Journal of Lightwave Technology*, Vol. 20, No. 7, 1210–1218, 2002.
2. Hadley, G. R., "High-accuracy finite-difference equations for dielectric waveguide analysis II: Dielectric corners," *Journal of Lightwave Technology,* Vol. 20, No. 7, 1219–1231, 2002.
3. Li, L.-Y. and J.-F. Mao, "An improved compact 2-D finite-difference frequency-domain method for guided wave structures,"

IEEE Microwave and Wireless Components Letters, Vol. 13, No. 12, 520–522, 2003.

4. Yu, C.-P. and H. C. Chang, "Compact finite-difference frequency-domain method for the analysis of two-dimensional photonic crystals," *Optics Express*, Vol. 12, 1397–163, 2004.
5. Chang, H. W. and W. C. Cheng, "Analysis of dielectric waveguide termination with tilted facets by analytic continuity method," *Journal of Electromagnetic Waves and Applications*, Vol. 21, No. 12, 1653–1662, 2007.
6. Zhao, W., H. W. Deng, and Y. J. Zhao, "Application of 4-component compact 2-D FDFD method in analysis of lossy circular metal waveguide," *Journal of Electromagnetic Waves and Applications,* Vol. 22, No. 17–18, 2297–2308, 2008.
7. Kusiek, A. and J. Mazur, "Analysis of scattering from arbitrary configuration of cylindrical objects using hybrid FD mode-matching method," *Progress In Electromagnetics Research*, Vol. 97, 105–127, 2009.
8. Chang, H.-W., Y.-H. Wu and W.-C. Cheng, "Hybrid FD-FD analysis of crossing waveguides by exploiting both the plus and the cross structural symmetry," *Progress In Electromagnetics Research,* Vol. 103, 217–240, 2010.
9. Chang, H.-W. and Y.-H. Wu, "Analysis of perpendicular crossing dielectric waveguides with various typical index contrasts and intersection profiles," *Progress In Electromagnetics Research,* Vol. 108, 323–341, 2010.
10. Mittra, R. and U. Pekel, "A new look at the perfectly matched layer (PML) concept for the reflectionless absorption of electromagnetic waves," *IEEE Microwave and Guided Wave Letter,* Vol. 5, No. 3, 84–86, 1995.
11. Zheng, S., W.-Y. Tam, D.-B. Ge, and J.-D. Xu, "Uniaxial PML absorbing boundary condition for truncating the boundary of DNG metamaterials," *Progress In Electromagnetics Research Letters,* Vol. 8, 125–134, 2009.
12. Chang, H.-W., W.-C. Cheng, and S.-M. Lu, "Layer-mode transparent boundary condition for the hybrid FD-FD method," *Progress In Electromagnetics Research*, Vol. 94, 175–195, 2009.
13. Jo, C.-H., C. Shin, and J.-H. Suh, "An optimal 9-point, finite-difference, frequency-space, 2-D scalar wave extrapolator," *Geophysics*, Vol. 61, No. 2, 529–537, 1996.
14. Singer, I. and E. Turkel, "High-order finite difference method for the Helmholtz equation," *Computer Methods in Applied*

Mechanics and Engineering, Vol. 163, 343–358, 1998.

15. Singer, I. and E. Turkel, "Sixth order accurate finite difference schemes for the Helmholtz equation," *Journal of Computational Acoustics*, Vol. 14, 339–351, 2006.
16. Nabavi, M., M. H. K. Siddiqui, and J. Dargahi, "A new 9-point sixth-order accurate compact finite-difference method for the Helmholtz equation," *Journal of Sound and Vibration*, Vol. 307, 972–982, 2007.
17. Sutmann, G., "Compact finite difference schemes of sixth order for the Helmholtz equation," *Journal of Computational and Applied Mathematics*, Vol. 203, 15–31, 2007.
18. Smith, G. D., *Numerical Solution of Partial Differential Equations, Finite Difference Methods*, 3rd edition, ISBN 19 859650 2, Glarendon Press, Oxford, 1985.
19. Hall, C. A. and T. A. Porsching, *Numerical Analysis of Partial Differential Equations*, 2nd edition, ISBN 9780136265573, Prentice Hall, Englewood Cliffs, NJ 07632, 1990.
20. Strikwerda, J. C., *Finite Difference Schemes and Partial Differential Equations*, 2nd edition, ISBN 0-89871-567-9, Siam, 2004.
21. Chang, H.-W. and S.-Y. Mu, "Novel nine-point FD coefficients for the two-dimensional Helmholtz equation," *Cross Strait Tri-Regional Radio Science and Wireless Technology Conference,* Hanan, China, 2010.
22. Nehrbass, J. W., J. O. Jevti'c, and R. Lee, "Reducing the phase error for finite-difference methods without increasing the order," *IEEE Trans. on Antennas and Propagation*, Vol. 46, No. 8, 1194–1201, 1998.
23. Burden, R. L. and J. D. Faires, *Numerical Analysis,* Brooks/Cole, Pacific Grove, CA, 2001.
24. Lehmann, T. M., C. Gonner, and K. Spitzer "Survey: Interpolation methods in medical image processing," *IEEE Transactions on Medical Imaging,* Vol. 18, No. 11, 1049–1075, 1999.
25. Elsherbeni, A. and V. Demir, *The Finite-difference Time-domain Method for Electromagnetics with MATLAB Simulations*, ISBN 9789746521048, SciTech Pub., Raleigh, NC 27615, 2009.
26. Ishimaru, A., *Electromagnetic Propagation, Radiation, and Scattering*, Prentice Hall, Englewood Cliffs, N.J., 1991.
27. Saleh, B. E. A. and M. C. Teich, *Fundamental of Photonics*, John Wiley & Son, New York, 1991.

28. Chang, H.-W., Y.-H. Wu, S.-M. Lu, W.-C. Cheng, and M.-H. Sheng, "Field analysis of dielectric waveguide devices based on coupled transverse-mode integral equation — Numerical investigation," *Progress In Electromagnetics Research,* Vol. 97, 159–176, 2009.
29. Chang, H.-W. and M.-H. Sheng, "Field analysis of dielectric waveguide devices based on coupled transverse-mode integral equation — Mathematical and numerical formulations," *Progress In Electromagnetics Research*, Vol. 78, 329–347, 2008.
30. Reiter, J. M. and F. Arndt, "Rigorous analysis of arbitrarily shaped H- and E-plane discontinuities in rectangular waveguides by a full-wave boundary contour mode-matching method," *IEEE Trans. on Microwave Theory and Techniques*, Vol. 43, No. 6, 796–801, 1995.
31. Kusiek, A. and J. Mazur, "Analysis of scattering from arbitrary configuration of cylindrical objects using hybrid FD mode-matching method," *Progress In Electromagnetics Research*, Vol. 97, 105–127, 2009.
32. Mohammad, R. Z, K. C. Donepudi, J.-M. Jin, and W. C. Chew, "Efficient time-domain and frequency-domain finite-element solution of Maxwell's equations using spectral Lanczos decomposition method," *IEEE Trans. on Microwave Theory and Techniques*, Vol. 46, No. 8, 1141–1149, 1998.
33. Fan, Z., D.-Z. Ding, and R.-S. Chen, "The efficient analysis of electromagnetic scattering from composite structures using hybrid CFIE-IEFIE," *Progress In Electromagnetics Research B*, Vol. 10, 131–143, 2009.
34. Chiou, Y. P., Y. C. Chiang, and H. C. Chang, "Improved three-point formulae considering the interface conditions in the finite-difference analysis of step-index optical devices," *Journal of Lightwave Technology*, Vol. 18, No. 2, 243–251, 2000.